Author Manuscript

Author Manuscript

Author Manuscript

Author Manuscript

HHS Public Access

Author manuscript

Magn Reson Med. Author manuscript; available in PMC 2025 May 01.

Published in final edited form as:

Magn Reson Med. 2024 May ; 91(5): 1822–1833. doi:10.1002/mrm.30015.

Functional activation of pyruvate dehydrogenase in human brain using hyperpolarized [1-^{13}C]pyruvate

Maheen Zaidi[a], **Junjie Ma**[a,b], **Binu P. Thomas**[a,c], **Salvador Peña**[a], **Crystal E. Harrison**[a], **Jun Chen**[a], **Sung-Han Lin**[a], **Kelley A. Derner**[a], **Jeannie D. Baxter**[a], **Jeff Liticker**[a], **Craig R. Malloy**[a,c], **Brenda Bartnik-Olson**[d], **Jae Mo Park**[a,c,e,*]

[a.]Advanced Imaging Research Center, The University of Texas Southwestern Medical Center, Dallas, Texas, USA 75390

[b.]GE Precision Healthcare, Jersey City, New Jersey, USA 07302

[c.]Department of Radiology, The University of Texas Southwestern Medical Center, Dallas, Texas, USA 75390

[d.]Department of Radiology, Loma Linda University, Loma Linda, California, USA 92354

[e.]Department of Biomedical Engineering, The University of Texas Southwestern Medical Center, Dallas, Texas, USA 75390

Abstract

Purpose: Pyruvate, produced from either glucose, glycogen, or lactate, is the dominant precursor of cerebral oxidative metabolism. Pyruvate dehydrogenase (PDH) flux is a direct measure of cerebral mitochondrial function and metabolism. Detection of [^{13}C]bicarbonate in the brain from hyperpolarized [1-^{13}C]pyruvate using ^{13}C MRI provides a unique opportunity for assessing PDH flux *in vivo*. This study is to assess changes in cerebral PDH flux in response to visual stimuli using *in vivo* ^{13}C MRS with hyperpolarized [1-^{13}C]pyruvate.

Methods: From seven sedentary adults in good general health, time-resolved [^{13}C]bicarbonate production was measured in the brain using 90° flip angles with minimal perturbation of its precursors, [1-^{13}C]pyruvate and [1-^{13}C]lactate, to test the hypothesis that the appearance of [^{13}C]bicarbonate signals in the brain reflects the metabolic changes associated with neuronal activation. With a separate group of healthy participants (n = 3), the likelihood of the bolus-injected [1-^{13}C]pyruvate being converted to [1-^{13}C]lactate prior to decarboxylation was investigated by measuring [^{13}C]bicarbonate production with and without [1-^{13}C]lactate saturation.

Results: In the course of visual stimulation, the measured [^{13}C]bicarbonate signal normalized to the total ^{13}C signal in the visual cortex increased by 17.1 ± 15.9% (P = 0.017) whereas no significant change was detected in [1-^{13}C]lactate. ^{1}H BOLD fMRI confirmed the regional activation in the visual cortex with the stimuli. Lactate saturation decreased bicarbonate-to-pyruvate ratio by 44.4 ± 9.3% (P < 0.01).

*Correspondence to Jae Mo Park, Ph.D., 5323 Harry Hines Blvd. Dallas, Texas 75390-8568, jaemo.park@utsouthwestern.edu, Tel: +1-214-645-7206.

Disclosure/Conflict of Interest: J.M. is an employee of GE Healthcare. The other authors declare no competing interests.

Author Manuscript Author Manuscript Author Manuscript Author Manuscript

Conclusion: We demonstrated the utility of ^{13}C MRS with hyperpolarized [1-^{13}C]pyruvate for assessing the activation of cerebral PDH flux via the detection of [^{13}C]bicarbonate production.

Keywords

dissolution dynamic nuclear polarization; hyperpolarized pyruvate; brain activation; functional magnetic resonance spectroscopy; pyruvate dehydrogenase; bicarbonate

INTRODUCTION

A series of metabolic processes, including increases in blood flow, oxygen and glucose consumption, and oxidative phosphorylation, are associated with neuronal activation[1,2]. These processes are essential in meeting elevated energy needs for the required brain function. Conventional blood oxygen level-dependent (BOLD) fMRI detects the signal perturbation due to deoxygenation of hemoglobin, and has been the dominant methodology for studying brain function and activation[3]. However, since BOLD fMRI depends on metabolic changes which are several steps away from neuronal activation, it is susceptible to other physiological changes and artifacts, which can result in diluted signal sensitivity, Figure 1.

Pyruvate dehydrogenase (PDH), the enzyme that regulates pyruvate flux into the tricarboxylic acid (TCA) cycle, plays a critical role in regulating the metabolic processes involved in cerebral oxidative phosphorylation[4]. PDH flux, therefore, is a direct measure of cerebral mitochondrial function and metabolism. The advent of dissolution dynamic nuclear polarization (DNP) of ^{13}C-labeled pyruvate enabled *in vivo* assessment of oxidative phosphorylation in the mitochondria as the production of [^{13}C]bicarbonate from administered hyperpolarized [1-^{13}C]pyruvate is a biomarker of PDH flux[5]. High-resolution ^{13}C imaging of cerebral metabolism in rodents using hyperpolarized [1-^{13}C]pyruvate[6] and its recent translation to human studies[7–9] have reported that [^{13}C]bicarbonate is primarily produced in the cerebral cortex where the majority of neuron cell bodies are located. The absence or miniscule amounts of labeled metabolic products specific to pyruvate carboxylase in astrocytes supports that the detected [^{13}C]bicarbonate is predominantly produced from neurons[9–11]. Coupling neuronal metabolism with hyperpolarized bicarbonate has not been actively explored in preclinical models since the pyruvate metabolism is heavily impacted by the anesthetic condition[12–14], therefore, detection of *in vivo* [^{13}C]bicarbonate production in humans presents exciting opportunities to assess the activation of neuronal metabolism directly.

Despite the unrivaled signal amplification of DNP, reliable detection and precise quantification of time-varying hyperpolarized signals are still technically challenging, particularly for mitochondrial products such as [^{13}C]bicarbonate. Previous imaging studies reported inconsistent and largely variable measurement of cerebral [^{13}C]bicarbonate production relative to the [1-^{13}C]pyruvate signal in the human brain[7,8]. This variability could be due to the biological variability among individuals such as baseline PDH activity, cerebral transport of hyperpolarized pyruvate, or the momentary difference in activation of the brain regions that were sampled. However, it is also possible that the large variation is

Author Manuscript Author Manuscript Author Manuscript Author Manuscript

attributed to the difficulty of reliably imaging [^{13}C]bicarbonate in the human brain. Dynamic MRS in combination with RF receive arrays has demonstrated robust regional detection of time-resolved hyperpolarized [^{13}C]bicarbonate in human brains[9]. However, dynamic ^{13}C MRS of hyperpolarized signals using a constant flip angle limits the RF sampling of product peaks at each timepoint and carries over the remaining "unsampled" signals to the next timepoint, making the sectional quantification of the products complicated. Moreover, lactate may play a significant role in the production of bicarbonate since the interconversion of pyruvate and lactate, catalyzed by the enzyme lactate dehydrogenase, is rapid and can occur before and after reaching brain tissues.

In this study, we demonstrate changes of bicarbonate production in response to visual stimuli in healthy volunteers and investigate the metabolic pathways to [^{13}C]bicarbonate formation from hyperpolarized [1-^{13}C]pyruvate in the brain, considering [1-^{13}C]lactate as a precursor.

METHODS

Study Participants

Ten healthy volunteers (age: 35.5 ± 14.1; body mass index = 25.3 ± 2.9; five male and five female) were recruited by word-of-mouth, Table 1. The protocol of this study is fully compliant with the HIPAA regulation, was approved by the Institutional Review Board (IRB) of The University of Texas Southwestern Medical Center (IRB#: STU 072017–009, STU-2018–0013). Written informed consent was obtained from the study participants. All participants tolerated the procedure without any incident.

Integrated ^{13}C/^{1}H MR Protocol

All studies were performed using a clinical 3T wide-bore MRI scanner (750w Discovery; GE Healthcare, Waukesha, Wisconsin, USA). Each participant underwent a ^{1}H/^{13}C-integrated MR protocol (45 – 60 min), which includes ^{1}H BOLD fMRI, ^{1}H Magnetization-Prepared Rapid Acquisition Gradient Echo (MPRAGE), and two dynamic ^{13}C MRS with separate injections of hyperpolarized [1-^{13}C]pyruvate (pyruvate concentration = 250 mM, dose = 0.1 mmol/kg body weight, volume = 0.43 mL/kg, injection rate = 5 mL/s) with a 30-minute interval between the injections (Figure 2a). A ^{13}C/^{1}H dual-frequency head coil (Clinical MR Solutions, LLC, Brookfield, Wisconsin, USA) that consists of ^{1}H quadrature transmit and receive, ^{13}C quadrature transmit and 8-channel ^{13}C receive arrays was used for the study[9], Figure 2b.

Following a ^{1}H fast GRE localizer, B_0 inhomogeneity was inspected using ^{1}H 2D GRE (FOV = 240 mm × 240 mm, spatial resolution = 6.25 mm × 6.25 mm, slice thickness = 2 cm, #slices = 2, TEs = 2.80 ms, 6.10 ms) and the shim currents were retained for ^{13}C scans. Simultaneously with each pyruvate injection, time-resolved ^{13}C spectra were acquired from a brain slab in axial or oblique plane that included the visual cortex using a dynamic ^{13}C MRS sequence (TR = 4 s, spectral width = 10,000 Hz, spectral points = 4,096, slab thickness = 3 cm). The ^{13}C MRS acquisitions used a custom-designed spectral-spatial RF pulse to excite hyperpolarized metabolites with distinct flip angles. The ^{13}C acquisition

Author Manuscript Author Manuscript Author Manuscript Author Manuscript

center frequency was set to the *in vivo* [1-^{13}C]pyruvate resonance, which was calculated from the resonance frequency of water protons as described previously[15]. Between the two ^{13}C scans, a 2D ^{1}H BOLD fMRI (FOV = 240 mm × 240 mm, matrix size = 64 × 64, slice thickness = 5 mm, #slice = 24, TE = 28 ms, TR = 2 s, flip angle = 80°) with the visual stimuli and 3D ^{1}H MPRAGE images (FOV = 256 mm × 256 mm × 180 mm, matrix size = 256 × 256 × 90, TE = 3.8 ms, TR = 8.7 ms, preparation time = 38 ms, flip angle = 8°) were acquired. The BOLD fMRI and MPRAGE scans were repeated using a 24-channel ^{1}H head coil (GE Healthcare) for improved signal sensitivity.

Two spectral-spatial RF pulses were designed using the Spectral-Spatial RF Pulse Design Package[16] with the gradient constraints for the wide-bore system (amplitude ≤ 25 mT/m and slew rate ≤ 100 T/m/s). One RF pulse (RF1, pulse duration = 21.9 ms) excited 90° on bicarbonate, 5° on pyruvate and 10° on lactate and the other (RF2, pulse duration = 21.9 ms) was designed to excite 90° on bicarbonate, 5° on pyruvate, and 90° on lactate, Figure 2c.

Experiments with Visual Stimuli

A subgroup of the participants (#1 - #7) was exposed to visual stimulation paradigm using a block design of circular blue/yellow checkerboards (4 Hz, stimulation ON; duration = 20 s) that alternated with a black screen with a cross in the center (stimulation OFF; duration = 20 s) during one of the ^{13}C MRS scans, Figure 2d. This paradigm was followed to maximize activation and the power for detection of the response to stimulation[17]. The ^{13}C brain slab was prescribed to include the visual cortex. As the scan started, the block-designed screen started playing. The second pyruvate injection was performed without the visual stimulation. RF1 was used for both the ^{13}C MRS. The same stimuli (4 min) were applied to ^{1}H BOLD fMRI and ^{13}C MRS for consistent stimulation. The dual-frequency ^{1}H/^{13}C RF head coil with 8-channel ^{13}C receive array was used during the first 45 minutes of the scan session. The BOLD fMRI and MPRAGE scans were repeated using a 24-channel ^{1}H head RF coil (GE Healthcare) for improved signal sensitivity.

Experiments with Lactate Saturation

^{13}C MRS from the other subgroup (participants #8 - #10) were acquired using RF1 and RF2 to assess the lactate saturation effect without the stimuli. The dual-frequency ^{1}H/^{13}C RF head coil was used throughout the experiment.

Hyperpolarization of [1-^{13}C]Pyruvate

Preparation and injection of hyperpolarized [1-^{13}C]pyruvate were performed as documented in the Investigational New Drug approval by the Food and Drug Administration (IND#: 133229). Up to three pyruvate samples were simultaneously polarized for each subject using a clinical SPINlab™ polarizer (GE Healthcare). 1.47g of GMP-grade [1-^{13}C]pyruvic acid (>99%; Sigma Aldrich, St Louis, Missouri, USA), mixed with 27.7 mg of AH111501 EPA radical (Syncom, Groningen, Netherlands), was inserted into a clinical fluid path in a sterile environment and polarized for 3 – 4 hours until dissolved by 38 mL of sterile water at 130 °C. The dissolved pyruvate solution was immediately mixed with 36.5 mL of room temperature TRIS/NaOH media (333 mM/600 mM) and tested using a quality control (QC) device (GE Healthcare) prior to the injection. Pyruvate concentration (238.9 ± 5.6 mM),

Author Manuscript Author Manuscript Author Manuscript Author Manuscript

pH (7.7 ± 0.5), and residual radical (1.4 ± 0.7 μM) of the injectate were measured. In parallel to the QC analysis, the hyperpolarized pyruvate solution was transferred to the study participant for an intravenous injection (transfer time = 56.4 ± 6.6 s).

^{13}C Data Reconstruction and Analysis

Dynamic ^{13}C MRS were reconstructed from the GE MR raw data using MATLAB R2021b (Mathworks, Natick, Massachusetts, USA) as described previously[18]. For assessing metabolic responses to visual stimuli (participants #1 – #7), ^{13}C data from channels #2 and #3 of the ^{13}C receive arrays were selectively combined and analyzed due to the proximity to the visual cortex. For comparing the RF pulses (participants #8 – #10), data from all ^{13}C channels were combined. Metabolite peaks, [^{13}C]bicarbonate, [1-^{13}C]lactate, and [1-^{13}C]pyruvate, were quantified from phase-corrected ^{13}C spectra by integrating the corresponding peak in absorption mode. The total ^{13}C signal, which was used to normalize [^{13}C]bicarbonate and [1-^{13}C]lactate peaks, was calculated by summing [^{13}C]bicarbonate, [1-^{13}C]lactate, and [1-^{13}C]pyruvate signals. For display purposes, the baseline was subtracted from the time-averaged spectra (0 – 160 s) by fitting a spline to the signal-free regions of the smoothed spectrum and normalized by the [1-^{13}C]pyruvate peak.

BOLD fMRI Analysis

All the BOLD fMRI data were analyzed using the Statistical Parametric Mapping Software version 12 (SPM12; Functional Imaging Laboratory, University College London, London, UK). In order to eliminate the possibility of potential motion artifacts during acquisition, each dataset in the NIfTI-1 format was first realigned by registering the 144 images to the first image in the series using a least-squares approach and a six-parameter spatial transformation. The realigned images were then normalized to the Montreal Neurological Institute (MNI) template space and convolved with a Gaussian kernel of a full width at half maximum of 8 mm isotropically.

Statistical Analysis

Data are presented as mean ± standard deviation. Statistical significance of changes in hyperpolarized ^{13}C metabolite signals between injections was evaluated by paired t-tests ($\alpha = 0.05$, two-tailed), assuming the normality of hyperpolarized ^{13}C metabolite signals and metabolite ratios[19,20]. Indeed, Miller, *et al.* showed that distribution of metabolite ratios is approximately normally distributed in the high signal-to-noise ratio regime (SNR > 10)[20]. The normality of ^{13}C metabolic ratios was also confirmed in a brain tumor patient study[19]. For statistical analysis of the fMRI data, model specification was performed on each individual subject's images using a 1st-level mass-univariate method based on general linear models with the masking threshold of 0.8. A brain activation map was generated using the contrast comparison between checkerboard stimulation and rest. Then, to acquire the mean activation of all subjects, a one-sample t-test in 2nd-level analysis was performed on the smoothed images. The mean activation clusters were generated for $P < 0.05$ and superimposed on the SPM12 canonical brain atlas (avg152T2).

Author Manuscript Author Manuscript Author Manuscript Author Manuscript

RESULTS

Participants in the first subgroup showed increased bicarbonate productions in the posterior ^{13}C coil components (channel #2 and #3) while viewing the checkerboard stimulus, as compared to those measured without the checkerboard stimuli, Figure 3a. The averaged BOLD response to the visual stimuli is shown in Figure 2b. Bicarbonate signal intensity (bicarbonate normalized to the total ^{13}C signal) in time-averaged (0 – 160 s) ^{13}C spectra increased by 17.1 ± 15.9 % from 0.154 ± 0.068 at rest to 0.178 ± 0.081 with the stimuli (P = 0.017), Figure 3b. Lactate normalized to the total ^{13}C signal also mildly increased from 0.310 ± 0.072 to 0.321 ± 0.075 (P = 0.064). The peak SNR of each metabolite in the time-averaged ^{13}C spectrum was 138 ± 52 for [^{13}C]bicarbonate (n = 14), 186 ± 68 for [1-^{13}C]lactate, and 438 ± 223 for [1-^{13}C]pyruvate. The pyruvate time-courses were comparable between the two injections, but time-advanced [1-^{13}C]pyruvate appearance was detected from some of the participants (#1, #4, #5) at the onset of the first stimulus beginning at 20 s, Figure 3c. During the first stimulus, the overall [^{13}C]bicarbonate signal was elevated (Figure 3d) but [^{13}C]lactate signal was maintained or increased by smaller amount from selected participants (#1, #3, #4, #5). The largest signal increase was detected at 4.6 ± 2.8 s from the start of the stimulus for [1-^{13}C]lactate and 5.1 ± 2.0 s for [^{13}C]bicarbonate. Signal changes during the subsequent stimuli presentation were under the detection limit.

Time-resolved ^{13}C spectra were acquired from the second subgroup with two consecutive injections of hyperpolarized [1-^{13}C]pyruvate using two different RF pulses. A larger [^{13}C]bicarbonate signal was detected using RF1 without lactate saturation as shown in the time-averaged ^{13}C (Figure 4a) and the time-courses (Figure 4c,d). The measured bicarbonate-to-pyruvate ratio from time-averaged ^{13}C spectra was 0.549 ± 0.045 with RF1 and 0.307 ± 0.066 with RF2 (P = 0.0098), which is a decrease by 44.4 ± 9.3 %. The lactate-to-pyruvate ratio increased by 56.7 ± 5.7 % from 0.838 ± 0.281 with RF1 to 1.304 ± 0.400 with RF2 (P = 0.021), Figure 4b.

DISCUSSION

Pathway Analysis of Cerebral [^{13}C]Bicarbonate Production from Hyperpolarized [1-^{13}C]Pyruvate

Metabolic profiles of neurons and astrocytes are distinct in terms of utilizing energy substrates to maintain metabolic homeostasis and to adaptively support high energetic demands of neurons. Pyruvate, the end-product of glycolysis and the redox pair, lactate, play a pivotal role in oxidative metabolism in the brain. Any form of its primary substrates, including glucose, glycogen, and lactate, is converted to pyruvate prior to entering the mitochondria for oxidative metabolism.

Although metabolic processes of steady-state infused ^{13}C-labeled thermal (non-hyperpolarized) glucose or lactate have been studied using ^{13}C MRS over timeframes ranging from minutes to hours, the metabolism of bolus injected pyruvate or lactate in the hyperpolarization timescale has not been explored. While intracellular pyruvate is undoubtedly the direct precursor of bicarbonate, it has often been assumed that this

Author Manuscript Author Manuscript Author Manuscript Author Manuscript

bicarbonate is converted straight from an administered hyperpolarized pyruvate bolus. However, [1-^{13}C]lactate, another major product of hyperpolarized [1-^{13}C]pyruvate in the brain, can complicate this procedure. Unlike [^{13}C]bicarbonate whose production is mitochondrion-specific, bolus-injected pyruvate can be rapidly converted to lactate in red blood cells and other organs before reaching brain tissues, Figure 5. The significantly reduced [^{13}C]bicarbonate signals in the dynamic ^{13}C MRS obtained with lactate saturation confirms that [1-^{13}C]lactate generated from a [1-^{13}C]pyruvate bolus is a substantial contribution to [^{13}C]bicarbonate formation in the brain. Therefore, preserving hyperpolarization in [1-^{13}C]lactate in addition to [1-^{13}C]pyruvate is required for optimal detection of total [^{13}C]bicarbonate production. This observation is consistent with previous studies that saturated lactate prior to bicarbonate imaging[21–23].

Contribution of Neuronal Metabolism to [^{13}C]Bicarbonate Production

It has been proposed that glutamate stimulates astrocytes to increase aerobic glycolysis, followed by lactate shuttling to neurons[24]. According to this astrocyte-neuron lactate shuttle (ANLS) theory[25], lactate is produced from glucose or glycogen in astrocytes, released via monocarboxylate transporter 4 (MCT4), and transferred to neurons[26]. However, the ANLS hypothesis remains controversial as it does not fulfill critical stoichiometric requirements between glucose uptake, lactate synthesis and release, and neuronal oxidation[27]. An infusion study with [3-^{13}C]lactate reported that the relative lactate transport capacity of neurons and astroglia can exceed glucose oxidation rates and, therefore, creates a shared lactate pool[28]. Along with the lactate shuttle theory which describes the roles of lactate in delivery of substrates[29], the direct lactate diffusion concept supports that pyruvate and lactate are adequate substrates for monitoring neural metabolism and neuronal activity. In particular, at supraphysiological plasma lactate concentrations as seen with the injection of hyperpolarized pyruvate or lactate, it was estimated that the contribution of plasma lactate to brain metabolism via direct lactate transport can increase up to 60%[28]. Additionally, significantly smaller *in vivo* lactate permeability was reported in astrocytes than neurons when lactate was injected intravenously[30], supporting our observation that neurons are a significant source of [^{13}C]bicarbonate production during stimulation.

The association between neuronal activity and cellular metabolism was recently investigated using hyperpolarized [1-^{13}C]pyruvate *ex vivo* by Grieb, *et al.*[31]. In this study, hyperpolarized [^{13}C]bicarbonate and [1-^{13}C]lactate in rat cerebrum slices were monitored after blocking action potential generation and inhibiting ATP-synthase using tetrodotoxin and oligomycin, respectively, and reported that PDH activity, measured by [^{13}C]bicarbonate, in the cerebrum increased by 4.4-fold with tetrodotoxin and decreased by 7.4-fold with oligomycin. This study supports that neuronal activity affects PDH activity and, thus, production of [^{13}C]bicarbonate.

In Vivo Detection of Cerebral PDH Activation in Humans

Assessing PDH flux has several advantages over the conventional imaging approaches. As illustrated in Figure 1, a cascade of physiological, metabolic processes is involved in brain activation. When the brain activation triggers oxidative phosphorylation in the mitochondria, PDH activity and subsequent oxidative metabolism in neurons increase during

Author Manuscript Author Manuscript Author Manuscript Author Manuscript

stimulation[32,33]. The increased oxidative metabolism demands a continuous supply of oxygen and glucose to neurons and astrocytes, leading to an increase in cerebral blood flow (CBF), cerebral blood volume, and cerebral metabolic rate of oxygen consumption.

The combinational changes of these factors form the basis of BOLD fMRI. The BOLD signal originates from deoxygenated hemoglobin, which is highly paramagnetic, resulting in gradients in the magnetic field and appearing as changes in T_2* relaxation in MRI[3]. As an indirect detection of neuronal activities, BOLD fMRI has several outstanding limitations. For instance, the concentration of deoxygenated blood can fluctuate due to variances in blood pressure or blood volume, affecting the BOLD signal[34,35]. In addition, the vascular delay that occurs during the signal acquisition can underestimate the level of neural activity[36]. For proper interpretation of brain activity, uncoupling of the neurovascular response is necessary to adjust the effects of the hemodynamic response on BOLD fMRI[37]. The hemodynamic response (CBF) can be measured by positron emission tomography (PET) techniques but the complex kinetics and large background signals complicate the analysis[38].

PET techniques can be also used to measure metabolic changes associated with brain activation such as variances in the cerebral metabolic rates of oxygen and glucose[39,40]. In particular, glucose utilization during the focal physiologic neural activity elicited by visual stimulation can be detected using ^{18}F-fluorodeoxyglucose PET[40]. However, cerebral glycogen metabolism needs to be uncoupled to accurately measure glucose oxidation resulting from stimulation. The glycogen shunt is a metabolic pathway that occurs in cells, in which glucose is converted into glycogen instead of being metabolized through the usual process of glucose oxidation[41]. In the brain, a fraction of glucose can be cycled through the cerebral glycogen pool and this cycling can increase with the degree of brain activation[42]. To measure glucose oxidation in the brain, it is necessary to uncouple the glycogen shunt by different methods such as inhibiting the enzymes involved in glycogen synthesis or depleting the glycogen stores.

In contrast, PDH activation is a direct measure of neuronal activity[43] that is not affected by the blood oxygen level. As a surrogate biomarker of PDH activity, the stimulus-triggered elevation of [^{13}C]bicarbonate production in the visual cortex suggests that the change reflects increased PDH flux due to neuronal activation. Although immediate increases in [^{13}C]bicarbonate production to the stimuli were detected in our study, further studies with faster sampling schemes would be necessary to investigate whether the metabolic change occurs prior to the hemodynamic response.

Several studies reported limited cellular transport of pyruvate. Rao, *et al.* reported that hyperpolarized [1-^{13}C]pyruvate-to-[1-^{13}C]lactate conversion rates are primarily a functional readout of [1-^{13}C]pyruvate transmembrane influx mediated by MCT1[44], an isoform that is mainly detected on endothelial cell of the blood-brain barrier (BBB). Indeed, opening the BBB facilitated cellular transport of hyperpolarized pyruvate and lactate to the brain[45–47]. In particular, Hackett, *et al.* demonstrated increased production of [^{13}C]bicarbonate and [1-^{13}C]lactate in the brain from hyperpolarized [1-^{13}C]pyruvate after opening the BBB with focused ultrasound[47]. Thus, it is possible that [^{13}C]bicarbonate production is already

Author Manuscript Author Manuscript Author Manuscript Author Manuscript

saturated without additional activation. However, MCT expression is regulated in relation to brain activity[48]. In a neural-derived cell line, both MCT1 and MCT4 are upregulated in hypoxia[49]. When the brain activation upregulates PDH activity and subsequent oxidative metabolism in the TCA cycle, the elevated PDH activity increases the uptake of lactate (and pyruvate) whose cellular transport is via MCT1 to astrocytes and via MCT2 to neurons[50–52].

Cerebral Lactate Production

Our study with the second subgroup focused on identifying the source of [^{13}C]bicarbonate in the brain. The result showed that [^{13}C]bicarbonate decreased by 44 % when lactate was saturated, suggesting that [1-^{13}C]lactate produced outside or inside the brain contributes approximately 56 % of [^{13}C]bicarbonate. Whether the [1-^{13}C]lactate produced outside the brain is the dominant source of [1-^{13}C]lactate in the brain is uncertain. An experimental setup such as having a lactate saturation band right outside of the brain (e.g., neck) prior to assessing brain metabolism would estimate the amount of [1-^{13}C]lactate production from [1-^{13}C]pyruvate in the brain.

Mixed results have been reported in terms of the change in lactate content by visual stimulation[53–56]. Our study showed an increasing trend of hyperpolarized [1-^{13}C]lactate during visual stimuli but the change was not as obvious as that seen in [^{13}C]bicarbonate. This is possibly due to the small flip angle excitation used for lactate and the increased [1-^{13}C]lactate delivery to the visual cortex by the elevated hemodynamic response. Further investigation is needed for quantitative investigation of functional changes in lactate.

Limitation and Future Improvement

This proof-of-concept study was performed with a limited number of subjects, and a larger cohort study may characterize functional metabolic changes better, depicted by hyperpolarized ^{13}C metabolites, with enhanced statistical power. The demonstrated method has several technical limitations that should be considered for future studies. First, a short observation window is an innate methodological limitation of the functional ^{13}C MRS with hyperpolarized [1-^{13}C]pyruvate due to the use of a contrast agent that generates transient hyperpolarized signals. Despite the high hyperpolarization level of [1-^{13}C]pyruvate and the optimized acquisition protocol, detecting task-induced [^{13}C]bicarbonate change was not achievable approximately a minute after a [1-^{13}C]pyruvate injection, which may underestimate the true extent of neuronal activation.

Second, data acquisition scheme can be further optimized to improve detection. The acquisition scheme of fully exciting hyperpolarized products at each dynamic time point was introduced for estimating metabolic exchange rates[57] and metabolic reaction rates[58]. In our study, the MR acquisition parameters were to reliably detect the relevant ^{13}C signals in the brain: [1-^{13}C]pyruvate, [1-^{13}C]lactate, and [^{13}C]bicarbonate. While bicarbonate was fully RF-sampled at each timepoint with a 90° excitation to measure produced bicarbonate signal during the time interval between the timepoint and the previous measurement, pyruvate and lactate were sampled with small flip angles to prevent their signals from being destroyed prior to the bicarbonate conversion. The flip angles of 5° and 10° were used for pyruvate and lactate, respectively, considering that hyperpolarized probes in injectate are

Author Manuscript Author Manuscript Author Manuscript Author Manuscript

typically larger than their products. Although the acquisition scheme with the parameters worked successfully, identical flip angles for both precursors would simplify the analysis. With the demonstrated signal sensitivities, even smaller flip angles for the precursors may be plausible for reliable detection of their time-courses and would further improve the bicarbonate sensitivity.

Third, identifying the response time of PDH flux to stimuli was limited, primarily due to the low temporal resolution. Shortening the repetition time, however, would decrease the amount of produced bicarbonate between timepoints, resulting in a reduced sensitivity of [^{13}C]bicarbonate detection, and would require more frequent RF excitations, which would shorten the observation time window. These dynamic acquisition and RF sampling schemes need to be investigated sufficiently prior to establishing appropriate imaging strategies.

Another parameter that was not thoroughly explored in this study is the stimulus design. A 20 s stimulus duration and interval were to avoid saturation and fatigue of the visual system and were chosen based on previous BOLD fMRI study design[17,59]. Moreover, a 30-minute interval between the ^{13}C scans may not be long enough for a complete return of stimulated brain metabolism to baseline, requiring further investigations.

Finally, quantitative techniques may need to be improved for future studies. This study focused on [^{13}C]bicarbonate and [1-^{13}C]lactate, normalized to the total ^{13}C signal. Due to lacking polarization measurements, absolute signal changes were not included in the analysis, and therefore, any change in blood flow could not be identified. For this, it is necessary to normalize the raw signal intensities by compensating experimental parameters such as polarization level and transport time[18]. In addition, the RF sampling factors should be considered to improve precision. However, quantifying multi-compartmental distribution of partially sampled, time-varying pyruvate and lactate signals with unknown *in vivo* characteristics such as T_1 relaxation times remains challenging[60,61]. Kinetic analysis can be considered as a potential quantification approach, considering that changes in metabolic reaction rates in the brain were previously demonstrated for data acquired with the product-selective saturating scheme[58].

In conclusion, we demonstrated the utility of ^{13}C MRI with hyperpolarized [1-^{13}C]pyruvate for assessing the activation of cerebral PDH flux. Our observation of elevated [^{13}C]bicarbonate formation in the visual cortex directly from hyperpolarized [1-^{13}C]pyruvate or from its reduced form, [1-^{13}C]lactate, in response to visual stimulation establishes the metabolic basis of existing modalities used to assess neuronal metabolism such as BOLD fMRI and PET.

Funding:

This work was supported by the National Institutes of Health of the United States (R01 NS107409, P41 EB015908, P30 DK127984, S10 OD018468, S10 RR029119); the U.S. Army Medical Research Acquisition Activity (W81XWH2210485); Muscular Dystrophy Association (MDA963281).

Author Manuscript Author Manuscript Author Manuscript Author Manuscript

REFERENCES

1. Logothetis NK. What we can do and what we cannot do with fMRI. Nature. 2008;453(7197):869–878. [PubMed: 18548064]
2. Brown GG, Perthen JE, Liu TT, Buxton RB. A primer on functional magnetic resonance imaging. Neuropsychol Rev. 2007;17(2):107–125. [PubMed: 17468956]
3. Ogawa S, Lee TM, Kay AR, Tank DW. Brain magnetic resonance imaging with contrast dependent on blood oxygenation. Proc Natl Acad Sci U S A. 1990;87(24):9868–9872. [PubMed: 2124706]
4. Reed LJ. Regulation of mammalian pyruvate dehydrogenase complex by a phosphorylation-dephosphorylation cycle. Curr Top Cell Regul. 1981;18(7):95–106. [PubMed: 7273851]
5. Merritt ME, Harrison C, Storey C, Jeffrey FM, Sherry AD, Malloy CR. Hyperpolarized 13C allows a direct measure of flux through a single enzyme-catalyzed step by NMR. Proc Natl Acad Sci U S A. 2007;104(50):19773–19777. [PubMed: 18056642]
6. Mayer D, Yen YF, Takahashi A, et al. Dynamic and high-resolution metabolic imaging of hyperpolarized [1– 13C]-pyruvate in the rat brain using a high-performance gradient insert. Magn Reson Med. 2011;65(5):1228–1233. [PubMed: 21500253]
7. Grist JT, McLean MA, Riemer F, et al. Quantifying normal human brain metabolism using hyperpolarized [1– 13 C]pyruvate and magnetic resonance imaging. Neuroimage. 2019;189(September 2018):171–179. [PubMed: 30639333]
8. Gordon JW, Chen HY, Autry A, et al. Translation of Carbon-13 EPI for hyperpolarized MR molecular imaging of prostate and brain cancer patients. Magn Reson Med. 2019;81(4):2702–2709. [PubMed: 30375043]
9. Ma J, Pinho MC, Harrison CE, et al. Dynamic 13C MR spectroscopy as an alternative to imaging for assessing cerebral metabolism using hyperpolarized pyruvate in humans. Magn Reson Med. 2022;87(3):1136–1149. [PubMed: 34687086]
10. Yu ACH, Drejer J, Hertz L, Schousboe A. Pyruvate Carboxylase Activity in Primary Cultures of Astrocytes and Neurons. J Neurochem. 1983;41(5):1484–1487. [PubMed: 6619879]
11. Uthayakumar B, Soliman H, Bragagnolo ND, et al. Age-associated change in pyruvate metabolism investigated with hyperpolarized 13C-MRI of the human brain. Hum Brain Mapp. 2023;44(10):4052–4063. [PubMed: 37219519]
12. Marjańska M, Shestov AA, Deelchand DK, Kittelson E, Henry PG. Brain metabolism under different anesthetic conditions using hyperpolarized [1–13C]pyruvate and [2–13C]pyruvate. NMR Biomed. 2018;31(12):1–8.
13. Hyppönen V, Stenroos P, Nivajärvi R, et al. Metabolism of hyperpolarised [1–13C]pyruvate in awake and anaesthetised rat brains. NMR Biomed. 2022;35(2):1–10.
14. Josan S, Hurd R, Billingsley K, et al. Effects of isoflurane anesthesia on hyperpolarized 13C metabolic measurements in rat brain. Magn Reson Med. 2013;70(4):1117–1124. [PubMed: 23086864]
15. Ma J, Chen J, Reed GD, et al. Cardiac T2* measurement of hyperpolarized 13C metabolites using metabolite-selective multi-echo spiral imaging. Magn Reson Med. 2021;86(3):1494–1504. [PubMed: 33821504]
16. Larson PEZ, Kerr AB, Chen AP, et al. Multiband excitation pulses for hyperpolarized 13C dynamic chemical-shift imaging. J Magn Reson. 2008;194(1):121–127. [PubMed: 18619875]
17. Liang CL, Ances BM, Perthen JE, et al. Luminance contrast of a visual stimulus modulates the BOLD response more than the cerebral blood flow response in the human brain. Neuroimage. 2013;64(1):104–111. [PubMed: 22963855]
18. Park JM, Harrison CE, Ma J, et al. Hyperpolarized 13C MR spectroscopy depicts in vivo effect of exercise on pyruvate metabolism in human skeletal muscle. Radiology. 2021;300(3):626–631. [PubMed: 34156298]
19. Zaccagna F, McLean MA, Grist JT, et al. Imaging Glioblastoma Metabolism by Using Hyperpolarized [1–13C]Pyruvate Demonstrates Heterogeneity in Lactate Labeling: A Proof of Principle Study. Radiol Imaging Cancer. 2022;4(4):1–10.
20. Miller JJ, Cochlin L, Clarke K, Tyler DJ. Weighted averaging in spectroscopic studies improves statistical power. Magn Reson Med. 2017;78(6):2082–2094. [PubMed: 28127795]

Author Manuscript Author Manuscript Author Manuscript Author Manuscript

21. Xu T, Mayer D, Gu M, et al. Quantification of in vivo metabolic kinetics of hyperpolarized pyruvate in rat kidneys using dynamic 13C MRSI. NMR Biomed. 2011;24(8):997–1005. [PubMed: 21538639]
22. Bøgh N, Grist JT, Rasmussen CW, et al. Lactate saturation limits bicarbonate detection in hyperpolarized 13 C-pyruvate MRI of the brain. Magn Reson Med. 2022;88(3):1170–1179. [PubMed: 35533254]
23. Wespi P, Steinhauser J, Kwiatkowski G, Kozerke S. Overestimation of cardiac lactate production caused by liver metabolism of hyperpolarized [1–13C]pyruvate. Magn Reson Med. 2018;80(5):1882–1890. [PubMed: 29607535]
24. Pellerin L, Magistretti PJ. Glutamate uptake into astrocytes stimulates aerobic glycolysis: A mechanism coupling neuronal activity to glucose utilization. Proc Natl Acad Sci U S A. 1994;91(22):10625–10629. [PubMed: 7938003]
25. Bélanger M, Allaman I, Magistretti PJ. Brain energy metabolism: Focus on Astrocyte-neuron metabolic cooperation. Cell Metab. 2011;14(6):724–738. [PubMed: 22152301]
26. Magistretti PJ, Allaman I. Lactate in the brain: From metabolic end-product to signalling molecule. Nat Rev Neurosci. 2018;19(4):235–249. [PubMed: 29515192]
27. Dienel GA. Lack of appropriate stoichiometry: Strong evidence against an energetically important astrocyte–neuron lactate shuttle in brain. J Neurosci Res. 2017;95(11):2103–2125. [PubMed: 28151548]
28. Boumezbeur F, Petersen KF, Cline GW, et al. The contribution of blood lactate to brain energy metabolism in humans measured by dynamic 13C nuclear magnetic resonance spectroscopy. J Neurosci. 2010;30(42):13983–13991. [PubMed: 20962220]
29. Brooks GA. Review The Science and Translation of Lactate Shuttle Theory. Cell Metab. 2018;27(4):757–785. [PubMed: 29617642]
30. Mächler P, Wyss MT, Elsayed M, et al. In Vivo Evidence for a Lactate Gradient from Astrocytes to Neurons. Cell Metab. 2016;23(1):94–102. [PubMed: 26698914]
31. Grieb B, Uppala S, Sapir G, Shaul D, Gomori JM, Katz-Brull R. Curbing action potential generation or ATP-synthase leads to a decrease in in-cell pyruvate dehydrogenase activity in rat cerebrum slices. Sci Rep. 2021;11(1):1–12. [PubMed: 33414495]
32. Hall CN, Klein-Flügge MC, Howarth C, Attwell D. Oxidative phosphorylation, not glycolysis, powers presynaptic and postsynaptic mechanisms underlying brain information processing. J Neurosci. 2012;32(26):8940–8951. [PubMed: 22745494]
33. Rangaraju V, Calloway N, Ryan TA. Activity-driven local ATP synthesis is required for synaptic function. Cell. 2014;156(4):825–835. [PubMed: 24529383]
34. Hussein A, Matthews JL, Syme C, et al. The association between resting-state functional magnetic resonance imaging and aortic pulse-wave velocity in healthy adults. Hum Brain Mapp. 2020;41(8):2121–2135. [PubMed: 32034832]
35. Kalisch R, Elbel GK, Gössl C, Czisch M, Auer DP. Blood pressure changes induced by arterial blood withdrawal influence bold signal in anesthesized rats at 7 Tesla: Implications for pharmacologic MRI. Neuroimage. 2001;14(4):891–898. [PubMed: 11554808]
36. Drew PJ. Vascular and neural basis of the BOLD signal. Curr Opin Neurobiol. 2019;58:61–69. [PubMed: 31336326]
37. Pak RW, Hadjiabadi DH, Senarathna J, et al. Implications of neurovascular uncoupling in functional magnetic resonance imaging (fMRI) of brain tumors. J Cereb Blood Flow Metab. 2017;37(11):3475–3487. [PubMed: 28492341]
38. Villien M, Wey HY, Mandeville JB, et al. Dynamic functional imaging of brain glucose utilization using fPET-FDG. Neuroimage. 2014;100:192–199. [PubMed: 24936683]
39. Fox PT, Raichle ME. Focal physiological uncoupling of cerebral blood flow and oxidative metabolism during somatosensory stimulation in human subjects. Proc Natl Acad Sci U S A. 1986;83(4):1140–1144. [PubMed: 3485282]
40. Fox PT, Raichle ME, Mintun MA, Dence C. Nonoxidative glucose consumption during focal physiologic neural activity. Science. 1988;241(4864):462–464. [PubMed: 3260686]

Author Manuscript Author Manuscript Author Manuscript Author Manuscript

41. Shulman RG, Hyder F, Rothman DL. Cerebral energetics and the glycogen shunt: Neurochemical basis of functional imaging. Proc Natl Acad Sci U S A. 2001;98(11):6417–6422. [PubMed: 11344262]
42. Dienel GA. Does shuttling of glycogen - derived lactate from astrocytes to neurons take place during neurotransmission and memory consolidation ? J Neurosci Res. 2019;97(November 2018):863–882. [PubMed: 30667077]
43. Lu M, Zhu XH, Zhang Y, Mateescu G, Chen W. Quantitative assessment of brain glucose metabolic rates using in vivo deuterium magnetic resonance spectroscopy. J Cereb Blood Flow Metab. 2017;37(11):3518–3530. [PubMed: 28503999]
44. Rao Y, Gammon S, Zacharias NM, et al. Hyperpolarized [1–13C]pyruvate-to-[1–13C]lactate conversion is rate-limited by monocarboxylate transporter-1 in the plasma membrane. Proc Natl Acad Sci U S A. 2020;117(36):22378–22389. [PubMed: 32839325]
45. Takado Y, Cheng T, Bastiaansen JAM, et al. Hyperpolarized 13C Magnetic Resonance Spectroscopy Reveals the Rate-Limiting Role of the Blood-Brain Barrier in the Cerebral Uptake and Metabolism of l -Lactate in Vivo. ACS Chem Neurosci. 2018;9(11):2554–2562. [PubMed: 29771492]
46. Peeters TH, Kobus T, Breukels V, et al. Imaging Hyperpolarized Pyruvate and Lactate after Blood-Brain Barrier Disruption with Focused Ultrasound. ACS Chem Neurosci. 2019;10(5):2591–2601. [PubMed: 30873831]
47. Hackett EP, Shah BR, Cheng B, et al. Probing Cerebral Metabolism with Hyperpolarized 13C Imaging after Opening the Blood-Brain Barrier with Focused Ultrasound. ACS Chem Neurosci. 2021;12(15):2820–2828. [PubMed: 34291630]
48. Bergersen LH. Lactate transport and signaling in the brain: Potential therapeutic targets and roles in body-brain interaction. J Cereb Blood Flow Metab. 2015;35(2):176–185. [PubMed: 25425080]
49. Cheng C, Edin NFJ, Lauritzen KH, et al. Alterations of monocarboxylate transporter densities during hypoxia in brain and breast tumour cells. Cell Oncol. 2012;35(3):217–227.
50. Tekkök SB, Brown AM, Westenbroek R, Pellerin L, Ransom BR. Transfer of glycogen-derived lactate from astrocytes to axons via specific monocarboxylate transporters supports mouse optic nerve activity. J Neurosci Res. 2005;81(5):644–652. [PubMed: 16015619]
51. Chiry O, Pellerin L, Monnet-Tschudi F, et al. Expression of the monocarboxylate transporter MCT1 in the adult human brain cortex. Brain Res. 2006;1070(1):65–70. [PubMed: 16403470]
52. Halim ND, Mcfate T, Mohyeldin A, et al. Phosphorylation status of pyruvate dehydrogenase distinguishes metabolic phenotypes of cultured rat brain astrocytes and neurons. Glia. 2010;58(10):1168–1176. [PubMed: 20544852]
53. Prichard J, Rothman D, Novotny E, et al. Lactate rise detected by 1H NMR in human visual cortex during physiologic stimulation. Proc Natl Acad Sci U S A. 1991;88(13):5829–5831. [PubMed: 2062861]
54. Sappey-Marinier D, Calabrese G, Fein G, Hugg JW, Biggins C, Weiner MW. Effect of photic stimulation on human visual cortex lactate and phosphates using1H and31P magnetic resonance spectroscopy. J Cereb Blood Flow Metab. 1992;12(4):584–592. [PubMed: 1618937]
55. Frahm J, Krüger G, Merboldt KD, Kleinschmidt A. Dynamic uncoupling and recoupling of perfusion and oxidative metabolism during focal brain activation in man. Magn Reson Med. 1996;35(2):143–148. [PubMed: 8622575]
56. Katz-Brull R, Alsop DC, Marquis RP, Lenkinski RE. Limits on activation-induced temperature and metabolic changes in the human primary visual cortex. Magn Reson Med. 2006;56(2):348–355. [PubMed: 16791859]
57. Schulte RF, Sperl JI, Weidl E, et al. Saturation-recovery metabolic-exchange rate imaging with hyperpolarized [1–13C] pyruvate using spectral-spatial excitation. Magn Reson Med. 2013;69(5):1209–1216. [PubMed: 22648928]
58. Harris T, Uppala S, Lev-Cohain N, et al. Hyperpolarized product selective saturating-excitations for determination of changes in metabolic reaction rates in real-time. NMR Biomed. 2020;33(2):1–15.
59. Amaro E, Barker GJ. Study design in fMRI: Basic principles. Brain Cogn. 2006;60(3):220–232. [PubMed: 16427175]

Author Manuscript Author Manuscript Author Manuscript Author Manuscript

60. Kazan SM, Reynolds S, Kennerley A, et al. Kinetic modeling of hyperpolarized 13C pyruvate metabolism in tumors using a measured arterial input function. Magn Reson Med. 2013;70(4):943–953. [PubMed: 23169010]

61. Bankson JA, Walker CM, Ramirez MS, et al. Kinetic modeling and constrained reconstruction of hyperpolarized [1–13C]-pyruvate offers improved metabolic imaging of tumors. Cancer Res. 2015;75(22):4708–4717. [PubMed: 26420214]

Author Manuscript Author Manuscript Author Manuscript Author Manuscript

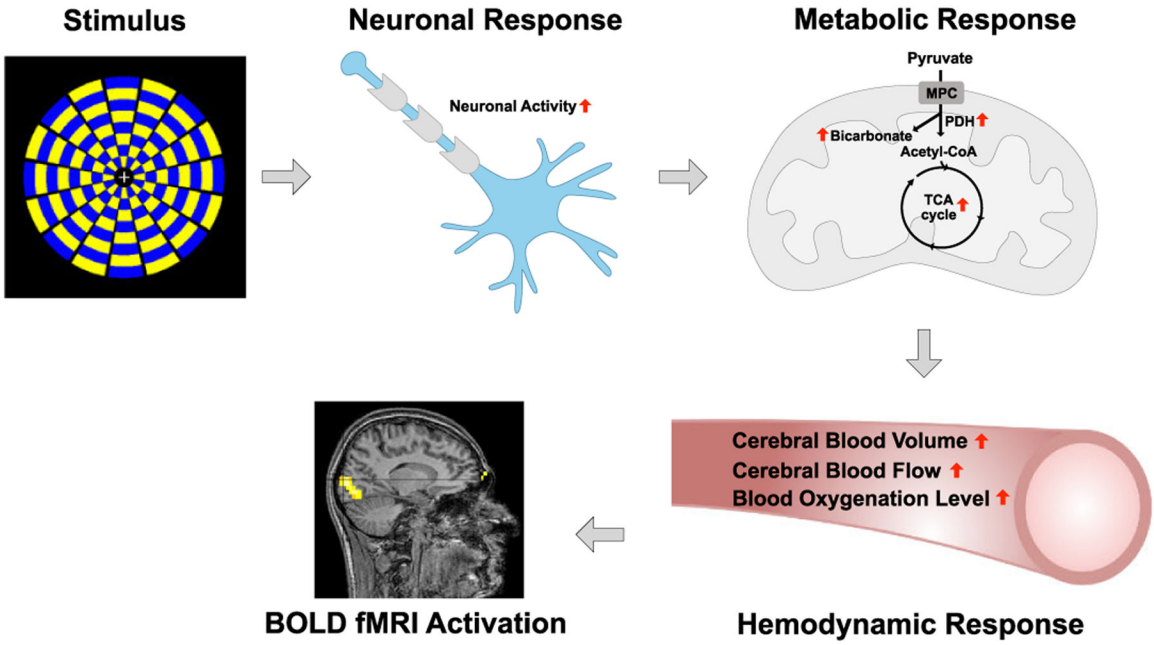

Figure 1. Functional Activation of Cerebral Metabolism.

In response to stimulation, oxidative metabolism and the activity of one of its key regulating enzymes, PDH, increase preceding concomitant changes in blood oxygen consumption, which results in changes in the BOLD signal. PDH: pyruvate dehydrogenase; BOLD: blood oxygen level dependent.

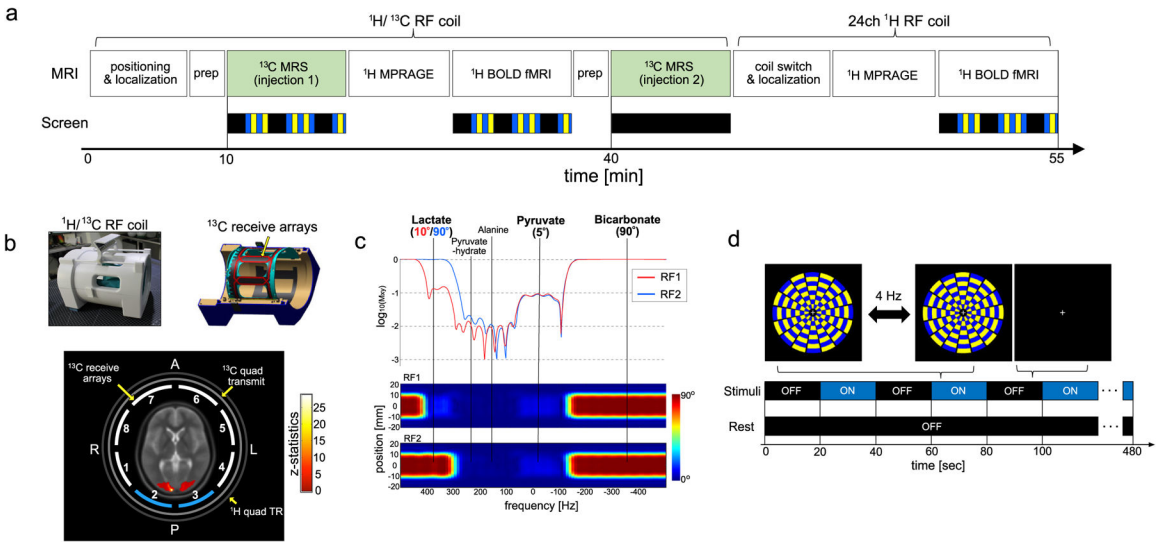

Figure 2. Experimental Protocol and Setup.

(a) The experimental MRI protocol that consists of ^{1}H BOLD fMRI, ^{1}H MPRAGE, and two dynamic ^{13}C MRS with hyperpolarized [1-^{13}C]pyruvate. (b) ^{13}C/^{1}H dual-frequency RF coil. Signals detected in the two posterior ^{13}C receive channels (colored in blue) of the ^{13}C/^{1}H dual-frequency RF coil were used to assess the metabolic changes due to visual stimulation. The activation map shown in the center of the coil is the averaged BOLD response to the visual stimuli. (c) Spectral-spatial excitation profiles of two RF pulses used to excite the [1-^{13}C]lactate resonance with 10° (RF1) and 90° (RF2) and their spectral profiles (RF1 as red line; RF2 as blue line) at the central position (z = 0). (d) ^{1}H BOLD fMRI and one of the ^{13}C MRS scans were acquired with block-designed checkerboard stimuli while the other ^{13}C MRS was without stimulation. AUC: area under the curve; BOLD: blood oxygenation level dependent.

Author Manuscript Author Manuscript Author Manuscript Author Manuscript

Author Manuscript Author Manuscript Author Manuscript Author Manuscript

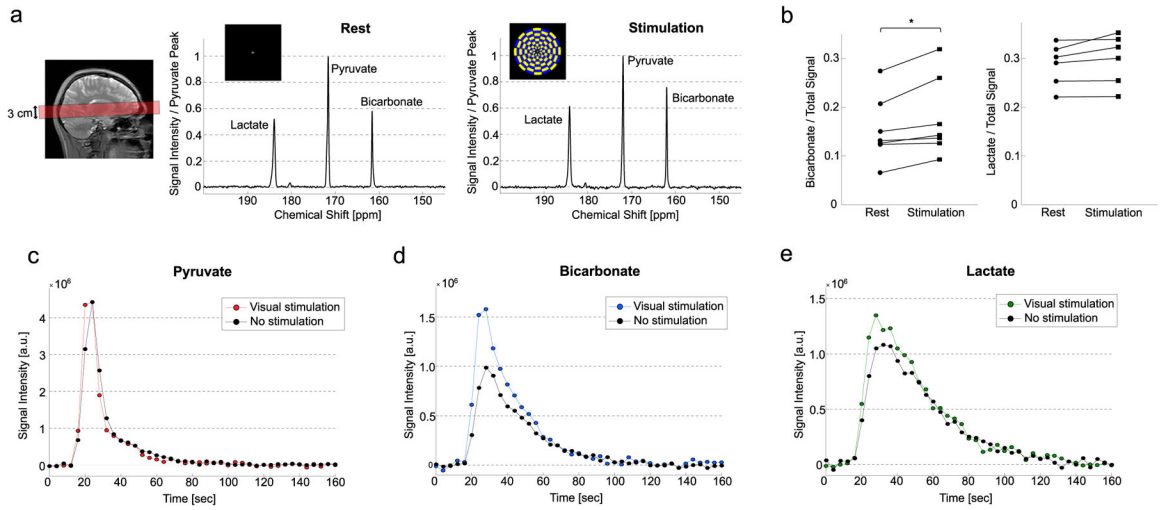

Figure 3. Activation of Pyruvate Dehydrogenase Flux in Response to Visual Stimulation.

(a) Time-averaged ^{13}C spectra acquired from a prescribed 3-cm slab that includes the visual cortex using the RF coil and the non-lactate-saturating RF pulse (RF1) with and without visual stimulation. (b) Bicarbonate AUC, normalized to the total ^{13}C signal, increased with the stimuli as compared to the baseline in all participants. The presented time-courses of hyperpolarized (c) [1-^{13}C]pyruvate, (d) [1-^{13}C]lactate, and (e) [^{13}C]bicarbonate signals with and without visual stimulation are from a representative participant (#1, 23 y.o. male). A coefficient was applied to the time-courses to match the maximum pyruvate signals between the injections. *: $P < 0.05$

Author Manuscript
Author Manuscript
Author Manuscript
Author Manuscript

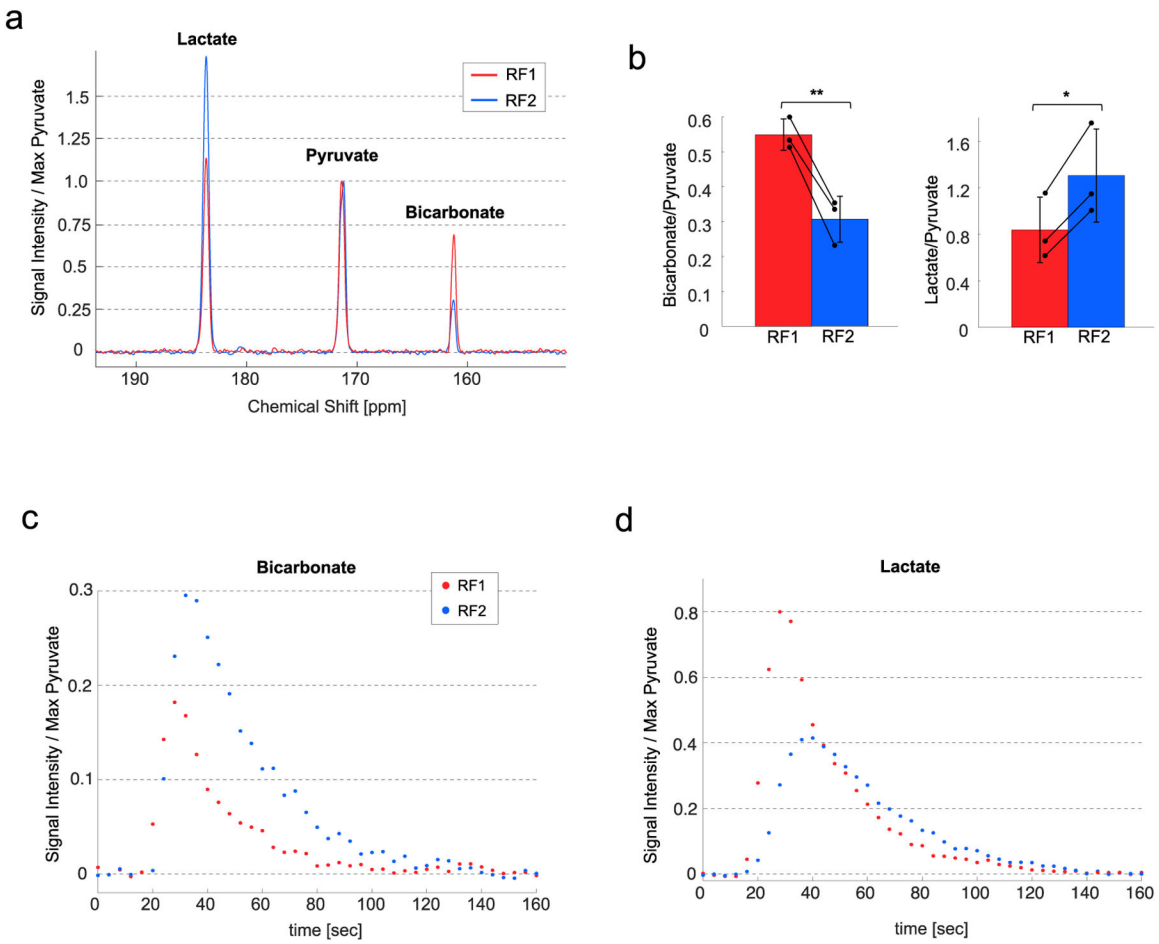

Figure 4. Effect of Saturating [1-^{13}C]Lactate on [^{13}C]Bicarbonate Formation.

(a) Time-averaged ^{13}C spectra from a representative healthy participant (#9, 32 y.o. male) using the RF pulses. (b) Decreased [^{13}C]bicarbonate and increased [1-^{13}C]lactate were measured with the lactate-saturating RF pulse (RF2) as compared to the measurements without lactate saturation (RF1). Time-courses of (c) [^{13}C]bicarbonate and (d) [1-^{13}C]lactate acquired from the participant. *: $P < 0.05$; **: $P < 0.01$

Author Manuscript Author Manuscript Author Manuscript Author Manuscript

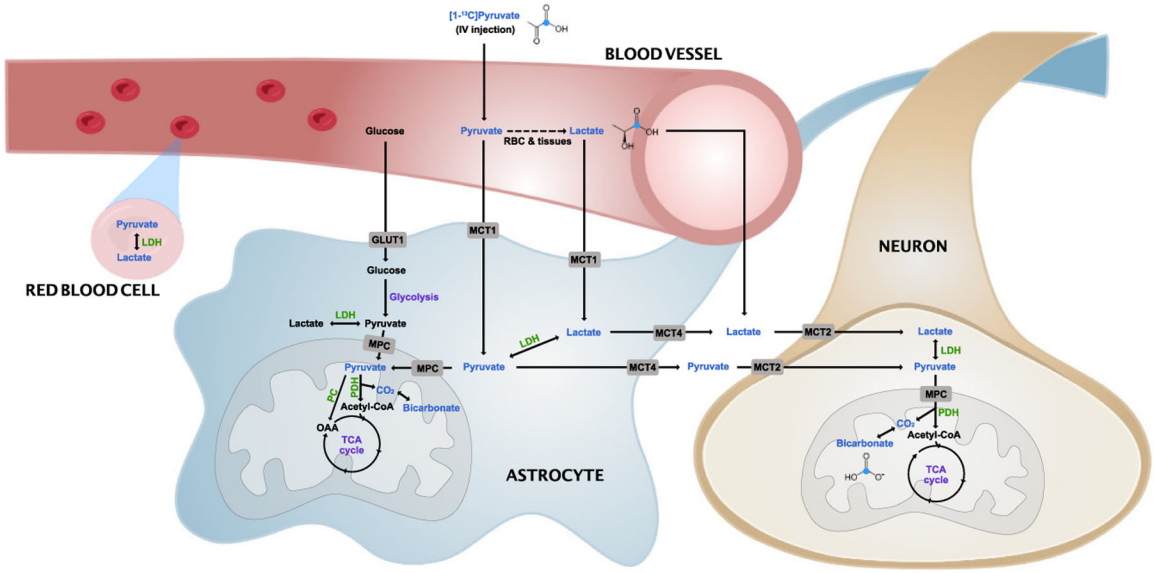

Figure 5. Pathway to Hyperpolarized [^{13}C]Bicarbonate Formation in The Brain.

Intravenously injected [1-^{13}C]pyruvate bolus can be converted to [1-^{13}C]lactate by red blood cells or other organs before being delivered to the brain. ^{13}C-labeled pyruvate and subsequent metabolic products are in blue font. GLUT: glucose transporter; LDH; lactate dehydrogenase; MCT: monocarboxylate transporter; MPC; mitochondrial pyruvate carrier; PC: pyruvate carboxylase; PDH: pyruvate dehydrogenase; RBC: red blood cell

Author Manuscript Author Manuscript Author Manuscript Author Manuscript

Table 1.

Study Participant Demographics.

Participant ID	Age [years]	Sex	Race	Ethnicity	BMI [kg/m^2]	Injection 1		Injection 2	
						RF pulse	Stimuli	RF pulse	Stimuli
1	23	M	Asian	Non-Hispanic	24.9	1	Visual	1	None
2	45	F	American Indian / Alaska Native	Non-Hispanic	27.7	1	Visual	1	None
3	22	F	Black/African American	Non-Hispanic	21.7	1	None	1	Visual
4	36	M	White	Non-Hispanic	25.2	1	Visual	1	None
5	21	M	White	Non-Hispanic	26.7	1	Visual	1	None
6	40	F	Black/African American	Non-Hispanic	23.0	1	None	1	Visual
7	26	M	White	Non-Hispanic	20.5	1	None	1	Visual
8	60	F	White	Non-Hispanic	29.4	1	None	2	None
9	32	M	White	Non-Hispanic	25.8	2	None	1	None
10	27	F	White	Hispanic	20.9	1	None	2	None